AIAA JOURNAL
Vol. 38, No. 9, September 2000

Influence of Nozzle Conditions and Discrete Forcing on Turbulent Planar Jets

S. A. Stanley*
Lawrence Berkeley National Laboratory, Berkeley, California 94720
and
S. Sarkar†
University of California, San Diego, La Jolla, California 92093-0411

Planar turbulent jets are of great interest in a broad range of engineering applications such as combustion, propulsion, and environmental flows. The influence of the turbulence intensity at the inflow and the shear-layer momentum thickness, as well as the effects of discrete forcing on the initial development of the jet, are studied computationally. It is found that the inflow fluctuation intensity and shear-layer momentum thickness have significant impact on the initial growth of the jet. Higher fluctuation intensity and thinner shear layers lead to more rapid growth of the jet with an asymptotic approach of the centerline turbulent kinetic energy to the self-similar values. The influence of the shear-layer thickness suggests a strong dependence of the initial growth on the shear-layer instabilities near the nozzle. Two-dimensional discrete forcing enhances the growth and two-dimensionality of the large-scale structures in the near field of the jet. However, significant three-dimensional small-scale structures coexist with the large-scale structures. The influence of the forcing is rapidly lost downstream as the large-scale structures break down.

Introduction

THE flowfield near the nozzle in planar turbulent jets is initially dominated by the shear layers at the jet edges. Michalke and Freymuth[1] showed that near the nozzle lip the most strongly growing disturbances are those corresponding to the shear layer. The shear layers spread downstream and interact to form a fully developed jet. Sato,[2] Rockwell and Niccolls,[3] as well as Antonia et al.,[4] showed that near the jet nozzle the large-scale structures in the flowfield are predominately symmetric for flat exit velocity profiles. When the shear layers interact downstream, these structures reorganize into an asymmetric configuration in the fully developed region of the jet. This reorganization as the flowfield develops from the shear layers near the nozzle to the fully developed jet downstream has a strong influence on the mixing in this region of the jet, which is not well understood.

Although the developing region of planar turbulent jets is of considerable engineering interest, most studies of turbulent plane jets have concentrated on the self-preserving region far downstream where the turbulence is fully developed. Bradbury,[5] Gutmark and Wygnanski,[6] and Ramaprian and Chandrasekhara,[7] as well as numerous others, measured statistical quantities in the self-preserving region while Oler and Goldschmidt,[8,9] Antonia et al.,[4] and Mumford[10] studied the organization of the large-scale structures in the fully developed region. Thomas and Goldschmidt,[11,12] Thomas and Chu,[13] and Thomas and Prakash[14] are perhaps the only researchers to concentrate on the study of the transition from the shear-layer dominated region near the nozzle to the fully developed region of the jet downstream. In general, however, they concentrated on the spectral development and reorganization of the large-scale structures. Thomas and Goldschmidt identified both symmetric and asymmetric modes in the near field of the jet and suggested that the asymmetric modes are caused by resonant forcing by the large-scale structures downstream. Thomas and Chu further confirmed the upstream feedback and suggested that it results from the loss of symmetry of the large-scale structures downstream of the end of the potential core. Finally, Thomas and Prakash studied the evolution from the shear layer modes near the nozzle to the jet column mode downstream in an untuned jet, where the subharmonic growth process in the shear layer is incapable of obtaining the jet mode. In other words, the fundamental frequency of the jet column mode f_{jt}^* is not related to the fundamental frequency of the shear-layer instability f_{sl}^* by a simple power of two, $f_{jt}^* \neq f_{sl}^*/2^n$.

Namer and Ötügen[15] performed an experimental study of the effects of Reynolds number on the initial development of the jet. They found that as the Reynolds number increases the jet develops more rapidly in the near field. They also observe stronger overshoots in the downstream development of the centerline turbulence intensities for lower-Reynolds-number jets. Hill and Jenkins[16] studied the effects of the nozzle exit velocity on the downstream evolution of the jet centerline velocity and the fluctuation intensity in the shear layer for nozzles with laminar and turbulent boundary layers. They found that with turbulent boundary layers the evolution of the jet is insensitive to variations in the nozzle exit velocity while with laminar boundary layers it is not. However, they did not determine whether the influence of the exit velocity (with laminar boundary layers) is caused by changes in the Reynolds number, or to variations in the nozzle conditions such as momentum thickness or fluctuation intensity.

Temporally and spatially evolving, two-dimensional plane jet simulations have been performed by Comte et al.[17] and Reichert and Biringen,[18] respectively. Dai et al.,[19] as well as Weinberger et al.,[20] performed large-eddy simulation of three-dimensional, spatially evolving plane turbulent jets using the Smagorinsky model, whereas Le Ribault et al.,[21] performed comparisons of three different large-eddy simulation models in these flows. However, to the authors' knowledge, no direct numerical simulation of three-dimensional, planar turbulent jets has been performed outside of the current study.

The purpose of this study is to characterize the influence of the jet nozzle conditions on the downstream evolution of the jet using direct numerical simulation (DNS). The effects of nozzle fluctuation intensity and shear-layer momentum thickness on the jet growth, centerline mean velocity decay, as well as centerline fluctuation intensity, are discussed next. In addition, the influence of symmetric and antisymmetric forcing at discrete frequencies on the evolution of the near field of the jet is studied.

Numerical Techniques

The unsteady, compressible, Navier–Stokes equations for an ideal gas are solved in the following form.

Received 23 April 1999; revision received 7 September 1999; accepted for publication 8 October 1999. This paper is declared a work of the U.S. Government and is not subject to copyright protection in the United States.

*Postdoctoral Fellow, Center for Computational Science and Engineering, 50A-1148. Member AIAA.

†Professor, Mechanical and Aerospace Engineering. Member AIAA.

Conservation of mass:

$$\partial_t \rho + \partial_i(\rho u_i) = 0 \tag{1}$$

Conservation of momentum:

$$\partial_t(\rho u_i) + \partial_j(\rho u_i u_j) = -\partial_i p + (1/Re)\partial_j \tau_{ij} \tag{2}$$

where

$$\tau_{ij} = (\partial_j u_i + \partial_i u_j) - \tfrac{2}{3}\delta_{ij}\partial_k u_k \tag{3}$$

and the equation for conservation of energy written as an evolution equation for the pressure

$$\partial_t p + u_i \partial_i p + \gamma p \partial_i u_i = (\gamma/PrRe)\partial_i \partial_i T + [(\gamma - 1)/Re]\tau_{ij}\partial_i u_j \tag{4}$$

The Euler terms in these equations are marched in time using the low-storage, fourth-order Runge–Kutta integration scheme of Carpenter and Kennedy.[22] This low-storage scheme requires only one additional array for each flowfield variable, thus reducing the memory requirements relative to the classical Runge–Kutta scheme. In addition, this is a five-stage scheme for which the additional stage is added to increase the overall stability of the scheme. Although this scheme does require an additional evaluation of the right-hand side of the governing equations, the relaxed stability criteria make the scheme 40% more efficient.

The viscous and conduction terms in Eqs. (1–4) are evaluated using a first-order integration scheme. This is implemented by advancing the Euler terms as just described and then evaluating and advancing the viscous and conduction terms with the first-order scheme. This technique requires 20% less computational work than advancing all of the terms using the Runge–Kutta scheme and has negligible impact on the results for the conditions of the jets in this study. The viscous and conduction terms are small compared to the advective terms and the Courant–Friedrichs–Lewy criterion requires a time step small enough so that first-order accuracy is sufficient.

A nonuniform fourth-order compact derivative scheme is used to evaluate the spatial derivatives. This scheme generalizes the uniform compact derivatives of Lele[23] to nonuniform meshes. This central derivative scheme is closed at the boundaries using inward biased, nonuniform, third-order compact derivatives based on the uniform derivatives of Carpenter et al.[24] The normal second-derivatives $\partial^2/\partial x^2$, $\partial^2/\partial y^2$, and $\partial^2/\partial z^2$ are evaluated using nonuniform, compact, second-derivative formulas, whereas the cross-derivative terms $\partial^2/\partial x \partial y$, etc., are evaluated using two successive applications of the first-derivative formulas. This compact 3-4-3 derivative scheme allows the simulation of problems on an open, nonperiodic, computational domain while maintaining an overall fourth-order accuracy on the nonuniform physical grid. Similar nonuniform compact schemes were analyzed by Gamet et al.[25]

All finite difference schemes generate their largest errors at the highest wave numbers supported by the computational grid $\kappa_x = 1/(2\Delta x)$. To eliminate these high wave-number errors, a nonuniform fourth-order compact filter is used. As with the nonuniform derivatives, the nonuniform compact filters generalize the uniform filters of Lele[23] and provide fourth-order accuracy in the physical grid spacing Δx. This filter is tuned to significantly affect only wave numbers $\kappa_x > 0.85/(2\Delta x)$ so that the filter does not remove dynamically significant scales of motion. All flowfield variables are filtered at the end of each time step. In the limit of a uniform grid, the nonuniform derivative scheme and computational filters go exactly to the uniform forms of Lele.

The computational grids used in this study are generated using a simple geometric progression $\Delta y_{i+1} = \Lambda_i \Delta y_i$, where Λ_i is the cell growth rate. In the streamwise (x) direction the grid is uniform $\Lambda = 1$, everywhere except in the buffer zone at the outflow. In the lateral (y) direction the grid is uniform in the region $-4.0h < y < 4.0h$ around the core of the jet, where h is the jet nozzle width at the inflow plane. Away from the core of the domain $|y| > 4.0h$, the stretching in the y direction is small, $\Lambda \leq 1.05$. In the spanwise (z) direction the grid is uniform throughout. For these grids the characteristics of the nonuniform derivative scheme and filters in the core of the domain are similar to those of the uniform schemes of Lele.[23] However, the nonuniform derivatives and filters properly allow for the small nonuniformity of the grid spacing while maintaining fourth-order accuracy.

One of the greatest difficulties in the simulation of spatially evolving flows is the formulation of the boundary conditions required for the open computational domain. In general, the flow occurs in an infinite or large physical domain; however, with simulations it is required to truncate the domain to the region of interest. During this truncation, information about the flowfield is lost. At the inflow boundary the governing equations are solved in a characteristic form. The time variation of the incoming characteristic variables are specified while the equation for the outgoing characteristic variable is solved using internal biased derivatives. This treatment of the inflow plane allows the jet to be forced with proper specification of the characteristic variables. In addition to this characteristic inflow forcing, a simple exponential damping term of the form

$$\partial_t(\rho u) = \text{Standard Terms} - \sigma_i(\rho u - \bar{\rho}\bar{u}) \tag{5}$$

is added to the streamwise momentum equation at the inflow plane. In this expression $\sigma_i = 0.22$ and $\bar{\rho}$ and $\bar{u}$ are the mean density and velocity profiles. These weak damping terms are added to neutralize the the long-time effects of the weak numerical diffusion, inherent in all high-order central difference schemes, on the inflow profiles. The weak damping terms coupled with the characteristic forcing provide steady mean profiles while allowing the desired fluctuation intensity about this mean.

For the downstream and sidewall boundaries the nonreflecting boundary conditions of Thompson[26, 27] are used. The form of these conditions is allowed to switch between nonreflecting inflow and outflow at each point on the boundary based on the sign of the instantaneous local normal velocity. The corner points on the outflow boundary are treated as nonreflecting at an angle 45 deg from the two adjacent boundaries. At all outflow points the pressure correction terms of Rudy and Strikwerda[28] and later discussed by Poinsot and Lele[29]:

$$\lambda_{\text{in}} n_k \partial_k W_{\text{in}} = K(p - p_\infty)/\rho c \tag{6}$$

where

$$K = \sigma_0 c\left(1 - M_{\max}^2\right)/L_y \tag{7}$$

are used in conjunction with the nonreflecting boundary conditions. In these expressions n_k is the normal to the boundary, W_{in} is the incoming characteristic variable, and λ_{in} is the propagation velocity. $M_{\max}$ is the maximum Mach number in the domain, L_y is the height of the domain in the y direction, c is the local speed of sound, and the constant $\sigma_0 = 0.25$. In the spanwise direction the domain is periodic.

In addition, a perfectly matched layer (PML) buffer zone based on that of Hu[30] is used on the sidewall and downstream boundaries to isolate further the interior of the domain from the effects of the boundary conditions. In this technique a region is added at the boundary in which the grid is stretched in the normal direction. In this stretched region exponential damping terms are added to the governing equations of the form (written for the density equation on a boundary whose normal is in the x direction)

$$\partial_t \rho = \text{Standard Terms} - \phi(x)(\rho - \bar{\rho}) \tag{8}$$

where

$$\phi(x) = \phi_m\left[(x - x^*)/L_b\right]^\beta \tag{9}$$

In these expressions x^* is the location of the interface between the buffer zone and the domain interior, and $L_b = x_{\max} - x^*$ is the length of the buffer zone. This term acts to damp the density to the specified value $\bar{\rho}$ across the buffer zone. Constant values of $\phi_m = 2.0$ and $\beta = 2.0$ are used on all three nonreflecting boundaries. On the sidewall boundaries the streamwise velocity is damped to the coflow velocity, whereas on the outflow boundary the streamwise velocity was damped to the profile of Bradbury[5]:

$$(U - U_2)/\Delta U_c = \exp\left\{-0.6749\left(y^2/\delta_U^2\right)\left[1.0 + 0.027\left(y^4/\delta_U^4\right)\right]\right\} \tag{10}$$

where δ_U is the jet half-width, U_2 is the coflow velocity, and $\Delta U_c = U(y = 0) - U_2$ is the centerline velocity excess. A target jet growth rate of $\delta_U/h = 0.1235(x/h - 0.873)$ is used, where h is

the jet nozzle width. The lateral velocity is damped to zero on the sidewall boundaries and to the profile given by the requirement that the mean field remains divergence free $\partial_i U_i = 0.0$ on the outflow boundary. The value of the centerline velocity excess ΔU_c in the outflow buffer zone is selected to maintain the same excess momentum flux:

$$J = \rho \int_{-\infty}^{\infty} U(U - U_2)\, dy \tag{11}$$

at the outflow plane as was present at the inflow. The spanwise velocity is damped to zero on all boundaries, and the pressure and density are damped to the constant inflow conditions. The grid stretching in the buffer zones is given by a simple geometric progression with a 5% stretching ratio.

The mean streamwise velocity profiles in the shear layers on either side of the jet at the inflow are given by a hyperbolic tangent profile:

$$u = (U_1 + U_2)/2 + [(U_1 - U_2)/2] \tanh[y_{sl}/(2\theta_0)] \tag{12}$$

where y_{sl} is the distance from the shear layer, θ_0 is the shear-layer momentum thickness, and U_1 and U_2 are the velocities of the high- and low-speed streams, respectively. This profile is mirrored across the centerline to obtain a top-hat profile with smooth edges. The mean lateral and spanwise velocities are zero at the inflow. The mean pressure and density profiles are uniform initially; however, a small variation across the jet is generated because of the outgoing acoustic waves.

Two types of forcing are used in the simulations discussed here, broadband and discrete. The broadband forcing is designed to provide energy to the flowfield in a range of scales characteristic of those present in an actual turbulent flow in order to increase the rate at which the jet evolves from the top-hat profiles present at the inflow to self-similar profiles downstream. This broadband forcing is performed by convecting a box of data past the inflow plane as the solution is integrated in time using a constant convection velocity $U_c = (U_1 + U_2)/2$. A sixth-degree interpolating polynomial is used to obtain the velocity, pressure, and density fields, which are then used to calculate the incoming characteristic variables. Forcing the inflow with a finite length time series in this way introduces a low-frequency component caused by the periodicity of the inflow data. However, with a carefully designed time series, such that the periodic frequency at the inflow is far from the dominant frequencies in the flowfield, this has minimal effect.

The box of data used in the broadband forcing is generated by first generating a pseudoisotropic velocity field u_i^{pi} with random phases and a three-dimensional energy spectrum given by

$$E(\kappa) = (\kappa^4/16) \exp\left[-2(\kappa/\kappa_0)^2\right] \tag{13}$$

The peak spatial frequency κ_0 is specified to be the fundamental mode for the hyperbolic tangent shear layer given by $\kappa_0^* \theta_0 = f^* \theta_0 / U_c = 0.033$ (Refs. 31 and 32), where f^* is the fundamental temporal frequency. A target vorticity field $\omega_i^t = \omega^{pi} S(y)$ is specified, where ω^{pi} is the vorticity field corresponding to the pseudoisotropic velocity field and $S(y)$ is a shape function that peaks in the shear layers on either side of the jet. The shape function $S(y) = \exp(-y_{sl}^2/\theta_0^2)$, mirrored across the jet in the same fashion as the mean velocity profile, is used to provide fluctuations that peak in the shear layer on either side of the jet. The velocity field corresponding to this target vorticity field is calculated by solving the Poisson equation $\partial_k \partial_k u_i^t = -\epsilon_{ijk} \partial_j \omega_k^t$ for each velocity component. This yields a divergence-free field. The corresponding pressure field is calculated by solving $\partial_k \partial_k p = -\rho \partial_j u_i \partial_i u_j$, and the density is specified by $\rho = p/c^2$, where c is the mean speed of sound. By calculating the density fluctuations in this way, the production of entropy at the inflow is reduced.

The discrete perturbations are added to the box of data used to force the inflow using the formulas

$$u^d = \sum_{\kappa_x,\, \phi_x} \frac{1}{\kappa_x} \left[\cos(y_{sl}) - \frac{2 y_{sl}}{\theta_0^2} \sin(y_{sl}) \right] \sin(\kappa_x x + \phi_x) \exp\left(-\frac{y_{sl}^2}{\theta_0^2}\right) \tag{14}$$

$$v^d = -\sum_{\kappa_x,\, \phi_x} \sin(y_{sl}) \cos(\kappa_x x + \phi_x) \exp\left(-\frac{y_{sl}^2}{\theta_0^2}\right) \tag{15}$$

and $w^d = 0$ for $(\kappa_x, \phi_x) = (\kappa_0^*, 0)$ and $(\kappa_0^*/2, \pi/2)$. The perturbations are mirrored symmetrically or asymmetrically across the jet centerline to provide the discrete forcing used in this study. Likewise, these expressions are rescaled to provide the desired forcing intensity.

Results and Discussion

The variation of the physical parameters for the simulations discussed here is given in Table 1. The parameter θ_0/h is the ratio of shear-layer momentum thickness to jet nozzle width, whereas $q_{bb}/\Delta U_0$ and $q_{disc}/\Delta U_0$ are the peak intensities of the broadband and discrete forcing at the inflow plane normalized by the inflow centerline velocity excess. All of these simulations are at an initial jet Reynolds number $Re_h = \rho h \Delta U_0/\mu = 3000$ and convective Mach number $M_c = \Delta U_0/(c_1 + c_2) = 0.16$. The final downstream values for case A are $Re_\delta = 2\rho\delta_U \Delta U/\mu = 4720$ and $M_c = 0.10$. Although these simulations are performed using the compressible Navier–Stokes equations, they are essentially incompressible because of the low convective Mach number. The velocity ratio $\eta = \Delta U_0/(U_1 + U_2)$ is 0.83, and the Prandtl number $Pr = C_p \mu/k = 0.72$.

All of the calculations in this study are performed on a grid of physical dimensions $L_x = 13.5h + 1.6h$, $L_y = 13.4h + 2.8h$, and $L_z = 4h$. This designation of $L = ah + bh$ indicates that the interior of the computational domain is of size ah with a buffer zone of size bh. For all cases except E, the computational grid is $205 \times 189 \times 60$, and the grid spacing in the interior of the computational domain is $\Delta x = \Delta y = \Delta z = 0.066h$. For case E the computational grid is $205 \times 277 \times 60$, and the grid spacing is $\Delta x = \Delta z = 0.066h$ and $\Delta y = 0.033h$. The finer grid spacing in the y direction is required to resolve the shear layer near the nozzle in this simulation.

Comparison with Experimental Data

Figure 1 shows the mean streamwise velocity profiles at several downstream stations for case A compared against the experimental data of Gutmark and Wygnanski[6] and Ramaprian and

Table 1 Inflow parameters

Case	θ_0/h	$q_{bb}/\Delta U_0$	$q_{disc}/\Delta U_0$
A	0.05	0.10	0.0
B	0.05	0.05	0.0
C	0.05	0.025	0.0
D	0.09	0.05	0.0
E	0.025	0.05	0.0
F	0.05	0.05	0.02 (symmetric)
G	0.05	0.05	0.02 (asymmetric)

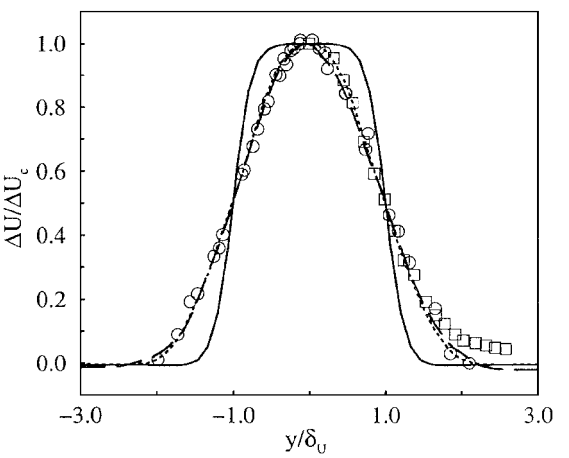

Fig. 1 Mean streamwise velocity profiles, case *A*: ——, *x/h* = 0.0; - - - -, *x/h* = 4.0; – – –, *x/h* = 11.5; □, Gutmark and Wygnanski[6]; and ○, Ramaprian and Chandrasekhara.[7]

Chandrasekhara.[7] The sharp initial shear-layer profiles can be seen for the station $x = 0.0h$. For this case the mean streamwise velocity profiles exhibit self-similarity for stations downstream of $x = 4.0h$. This station is very near the point at which the two shear layers on either side of the jet first merge. As can be seen, good comparison with experimental data for turbulent plane jets is observed.

Analysis of the self-similar region of planar turbulent jets predicts a linear relationship between the jet half-width δ_U and the downstream coordinate x:

$$\delta_U / h = K_{1u}(x/h - K_{2u}) \tag{16}$$

For case A the constants in this relationship are $K_{1u} = 0.095$ and $K_{2u} = -0.823$ based on the region $x \geq 7.5h$. The growth rates K_{1u} are a little low compared to the values of 0.100 of Gutmark and Wygnanski and 0.110 from Ramaprian and Chandrasekhara. The virtual origin K_{2u} is the physical location at which the linear fit in the fully developed region gives a zero jet width (the origin of a point momentum source giving the specified linearly growing jet). In general, there is a great deal of scatter in the values for K_{2u} because of their sensitivity to the conditions at the jet nozzle.

Analysis of the self-similar centerline velocity decay predicts an inverse-squared relationship between the centerline velocity excess ΔU_c and the downstream coordinate:

$$\left(\frac{\Delta U_0}{\Delta U_c}\right)^2 = C_{1u}\left(\frac{x}{h} - C_{2u}\right) \tag{17}$$

where ΔU_0 is the centerline velocity excess at the jet nozzle. The constants in this expression for case A are $C_{1u} = 0.212$ and $C_{2u} = 0.760$ (for $x \geq 7.5h$). The centerline velocity decay rate C_{1u} compares well with the experimentally observed values ranging from 0.093 (Ref. 7) to 0.220 (Refs. 13 and 14).

For brevity, only a limited comparison of these results against experimental data is discussed here. For a more detailed analysis of a single simulation, as well as a more complete comparison with the available experimental data, see Refs. 33 and 34.

The influence of grid resolution on these results has been analyzed by comparison against a simulation performed with 17% higher resolution $\Delta x = \Delta y = \Delta z = 0.055$ in the core of the domain. The observation was made that there was little impact on the evolution of the mean fields, self-similar growth rates, and centerline velocity decay rates. There were small changes in the local values of the fluctuation intensities; however, there was not a significant change in the general trends. Likewise, Stanley and Sarkar[35] studied the influence of domain size on the evolution of two-dimensional shear layers using the same boundary condition scheme used for this study. An increase in the length of the computational domain was found to influence only the region very near the boundary, and in this region the effect was small, $<4\%$. The impact on the three-dimensional simulations in this study will be even smaller because of the lack of strong large-scale structures. Truncation of the small-scale turbulence in this study has less impact on the solution than truncation of the two-dimensional vortex street.

Influence of the Inflow Fluctuation Intensity

In most experimental studies the fluctuation intensity at the jet nozzle is only reported on the centerline. However, because of the boundary layers upstream, the fluctuation intensity peaks in the shear layers on either side of the jet. Because the peak mean shear is also in the shear layers near the nozzle, it is clear that the fluctuation intensity in this region of the jet will have a strong influence on the initial downstream evolution. To characterize the influence of the fluctuation intensity on the initial development of planar jets, results from three simulations, cases A, B, and C, with different broadband intensities at the inflow plane are presented. It is believed that the broadband intensity in case C is relatively typical of that in experimental studies with laminar boundary layers while the broadband intensity in case A is closer to that which would occur in a jet exiting from a turbulent channel.

Figures 2 and 3 show the variation with broadband inflow forcing intensity of the evolution of the centerline mean velocity excess and the jet half-width, respectively. These figures clearly show that the inflow fluctuation intensity has a strong influence on the initial growth of the jet. When the inflow fluctuation intensity is increased from $q_{bb}/\Delta U_c = 0.025$ to 0.10, the length of the potential core, based on the constancy of the centerline mean velocity excess, decreases from $6h$ to $3h$. However, in the self-similar region downstream the jet grows at nearly the same rate, and the centerline velocity excess decays at nearly the same rate for all inflow fluctuation intensities.

Table 2 Variation of the jet growth and centerline velocity decay coefficients with inflow fluctuation intensity

Case	$q_{bb}/\Delta U$	K_{1u}	K_{2u}	C_{1u}	C_{2u}
A	0.10	0.095	−0.823	0.212	0.760
B	0.05	0.102	0.476	0.216	1.78
C	0.025	0.103	1.13	0.224	2.48

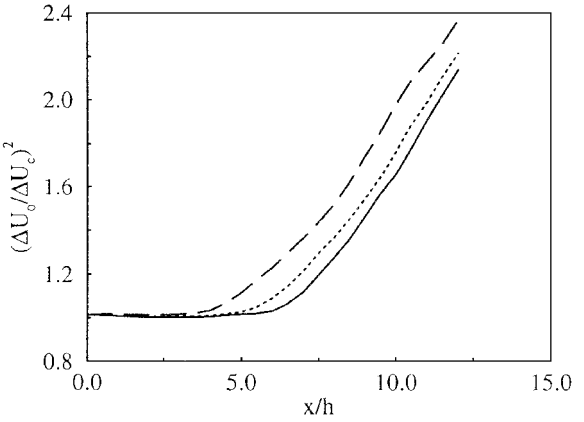

Fig. 2 Downstream evolution of the centerline velocity excess for different broadband inflow intensities: ——, $q/\Delta U = 0.025$; - - - -, $q/\Delta U = 0.05$; and – – –, $q/\Delta U = 0.10$.

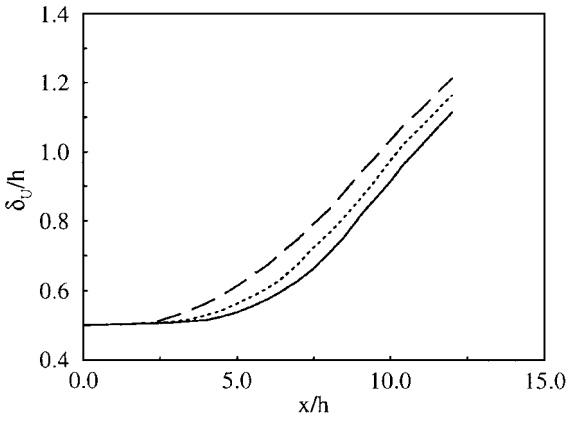

Fig. 3 Downstream evolution of the jet half-width for different broadband inflow intensities: ——, $q/\Delta U = 0.025$; - - - -, $q/\Delta U = 0.05$; and – – –, $q/\Delta U = 0.10$.

Table 2 gives the parameters for the self-similar fits of the jet half-width and the centerline mean velocity excess for all three cases. The stations $x \geq 7.5h$, $x \geq 8.0h$, and $x \geq 8.5h$ were used in these fits for cases A, B, and C, respectively. There is a strong upstream shift (more negative) in the virtual origins K_{2u} and C_{2u} for increasing inflow fluctuation intensity. This indicates a more rapid evolution to the linear behavior characteristic of the self-similar region of the jet. There is also a slight decrease in the jet growth rates K_{1u} and centerline velocity decay rates C_{1u}. Although this change is small, it is consistent across the range of $q_{bb}/\Delta U_c$ studied. Hussain and Zedan[36] observed a similar influence of the boundary-layer fluctuation intensity on the self-similar growth rates of axisymmetric turbulent shear layers. However, they observe that an increase in the fluctuation intensity produces shear layers with larger growth rates while we observe a small decrease in planar jets.

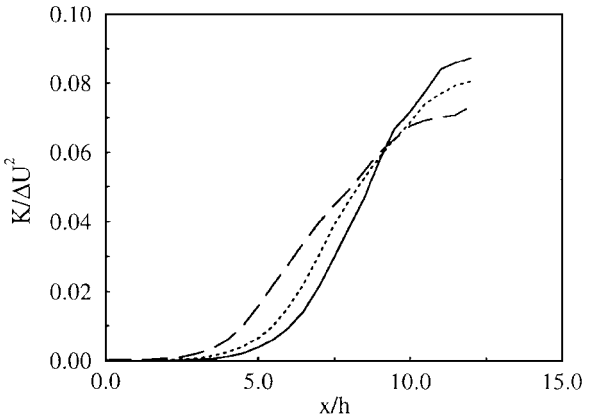

Fig. 4 Downstream evolution of the centerline turbulence intensity for different broadband inflow intensities: ——, $q/\Delta U = 0.025$; - - - -, $q/\Delta U = 0.05$; and – – –, $q/\Delta U = 0.10$.

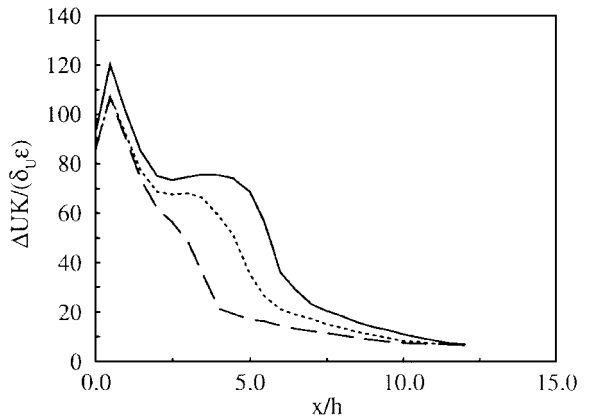

Fig. 5 Downstream evolution of the turbulent kinetic energy to dissipation ratio on the jet centerline for different broadband inflow intensities: ——, $q/\Delta U = 0.025$; - - - -, $q/\Delta U = 0.05$; and – – –, $q/\Delta U = 0.10$.

Figure 4 shows the variation of the downstream growth of the centerline turbulent kinetic energy with changes in the inflow fluctuation intensity. As expected, the initial growth of the centerline turbulent kinetic energy is more rapid for the highest inflow fluctuation intensity than for the smallest. The region of strong growth in the turbulent kinetic energy shifts from $\approx 3.5h$ to $\approx 7.0h$ with a decrease in the broadband forcing intensity from 0.10 to 0.025. However, near the outflow of the domain, the centerline turbulent kinetic energy for the cases with lower intensity inflow fluctuations exceeds the turbulent kinetic energy for the highest inflow fluctuation intensity. For $q_{bb}/\Delta U_0 = 0.10$ the centerline turbulent kinetic energy $K/\Delta U^2$ grows asymptotically to a value ≈ 0.07. Gutmark and Wygnanski[6] observed a centerline turbulent kinetic energy of 0.075 while Browne et al.[37] found 0.05. However for lower intensity fluctuations at the inflow, the centerline turbulent kinetic energy overshoots to values of 0.08 and 0.09 in the DNS. With a longer computational domain it is speculated that a slow decay would be observed downstream to the values more typical of turbulent planar jets.

Figure 5 shows the downstream evolution of the nondimensionalized ratio of the turbulent kinetic energy K to the dissipation ϵ on the jet centerline for these three simulations. This, $\Delta U K/\delta_U \epsilon$, is the ratio of the turbulence timescale to the mean-flow timescale. The evolution of this ratio is an indicator of the relative state of equilibrium of the turbulence. Near the inflow this ratio is large, small dissipation relative to the turbulent kinetic energy, indicating that the turbulence is highly nonequilibrium. Downstream, the dissipation grows relative to the turbulent kinetic energy, and this ratio approaches a value of ≈ 6.5 for all three inflow fluctuation intensities. For $q_{bb}/\Delta U_0 = 0.10$ the turbulent fields approach equilibrium quickly downstream in the jet as indicated by the rapid approach of $\Delta U K/(\delta_U \epsilon)$ to the equilibrium value. However, for the lower inflow fluctuation intensities the development of equilibrium turbulence is slower. This relatively larger region of nonequilibrium turbulence for smaller inflow fluctuation intensities allows the overshoot in the turbulent kinetic energy downstream in the jet.

Similar overshoots in the turbulent kinetic energy were observed by Namer and Ötügen[15] and Browne et al.[37] Namer and Ötügen also observed an influence of the jet Reynolds number on the overshoot in the turbulence intensities. They found that jets with lower initial Reynolds numbers Re_h developed larger overshoots in the centerline streamwise fluctuation intensity. A large overshoot was observed for a $Re_h = 1000$ jet, whereas for $Re_h = 7000$ no overshoot was observed in the streamwise fluctuation intensity.

Influence of the Shear-Layer Momentum Thickness

The momentum thickness of the shear layers at the jet nozzle are often quoted in studies of planar jets. However, no consistent study of the influence of the initial shear-layer thickness on the development of the jet has been performed. To understand the influence of the initial momentum thickness, three simulations have been performed with varying shear-layer thickness. Cases D, B, and E have initial momentum thicknesses θ_0 of $0.09h$, $0.05h$, and $0.025h$, respectively. The initial fluctuation intensity for all of these cases is $q_{bb}/\Delta U_0 = 0.05$.

Figures 6 and 7 show the effect of varying the shear-layer momentum thickness on the centerline mean excess velocity decay and the jet half-width. Although the shear-layer conditions are often ignored when comparing the evolution of jets from different studies, the current results demonstrate unequivocally that the shear-layer momentum thickness is an important parameter in the characterization of the initial region of planar turbulent jets. When the shear-layer momentum thickness decreases from $0.09h$ to $0.025h$, the length of the potential core of the jet based on the constancy of the centerline mean velocity excess decreases from $6.0h$ to $3.5h$. Likewise, there

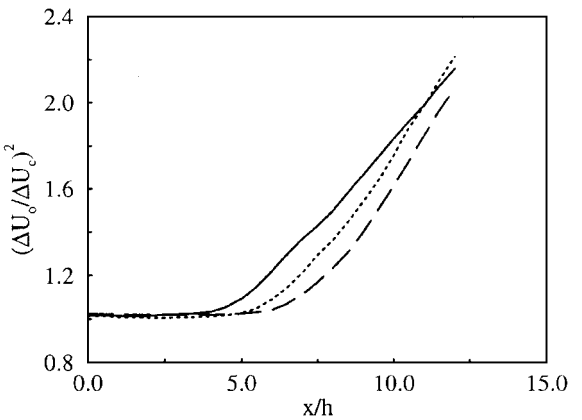

Fig. 6 Downstream evolution of the centerline velocity excess for different initial shear-layer momentum thicknesses: ——, $\theta_0/h = 0.025$; - - - -, $\theta_0/h = 0.05$; and – – –, $\theta_0/h = 0.09$.

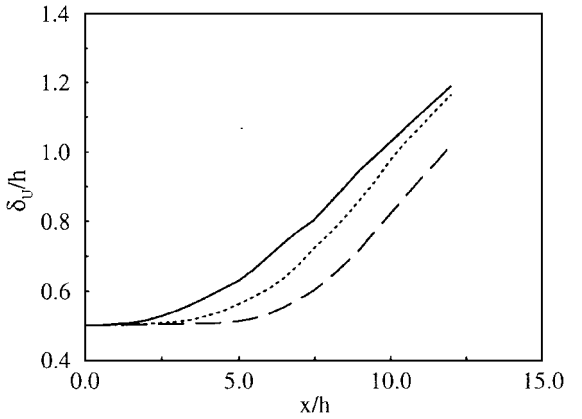

Fig. 7 Downstream evolution of the jet half-width for different initial shear-layer momentum thicknesses: ——, $\theta_0/h = 0.025$; - - - -, $\theta_0/h = 0.05$; and – – –, $\theta_0/h = 0.09$.

Table 3 Variation of the jet growth and centerline velocity decay coefficients with initial shear-layer momentum thickness

Case	θ_0/h	K_{1u}	K_{2u}	C_{1u}	C_{2u}
D	0.09	0.098	1.66	0.219	2.59
B	0.05	0.102	0.476	0.216	1.78
E	0.025	0.085	−2.08	0.162	−1.30

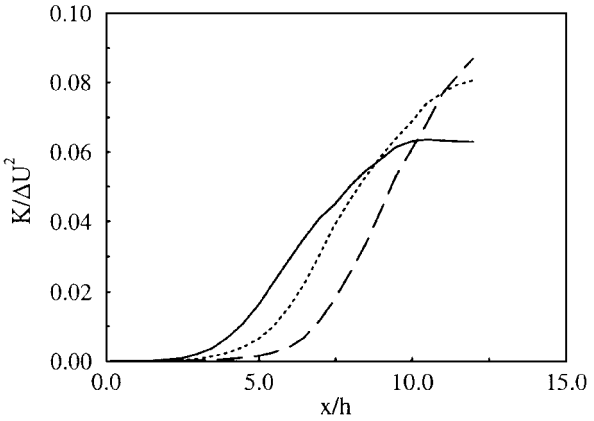

Fig. 8 Downstream evolution of the centerline turbulence intensity for different initial shear-layer momentum thicknesses: ——, $\theta_0/h = 0.025$; - - - -, $\theta_0/h = 0.05$; and – – –, $\theta_0/h = 0.09$.

is a strong shift in the location at which the jet width grows strongly from $6.0h$ to $2.0h$.

As just shown for the inflow fluctuation intensity, the decrease in the shear-layer momentum thickness is felt most strongly in the virtual origins in the self-similar fits of the jet half-width and the centerline velocity decay (Table 3). The stations $x \geq 7.5h$, $8.0h$, and $8.5h$ were used in these fits for cases E, B, and D, respectively. With a decrease in the momentum thickness, the mean velocity profiles evolve more rapidly to self-similar behavior resulting in an upstream shift in the virtual origins. There is also a significant influence of the inflow momentum thickness on the jet growth rates K_{1u} and centerline velocity decay rates C_{1u}. There is a 20% change in the jet growth rates and a 35% change in the centerline velocity decay rates over the range of momentum thickness studied. In contrast, there is only an 8% change in the growth rates and 6% change in the velocity decay rates for the range of inflow forcing intensity discussed earlier. Although the change in the centerline velocity decay rate is consistent across the range of momentum thickness, the change in the jet growth rate is not. In contrast, Hussain and Zedan[38] saw only a small 2% variation in the shear-layer growth rates with a factor-of-three increase in the initial momentum thickness.

The idea of the initial conditions modifying the downstream behavior is not new to this paper. George[39] pointed out that the initial conditions can influence the downstream behavior of the large-scale coherent structures in the flow. These structures will in turn affect the downstream growth rates and centerline decay rates.

Figure 8 shows the downstream evolution of the centerline turbulent kinetic energy for the three simulations. Decreasing the shear-layer momentum thickness has a similar influence on the centerline turbulent kinetic energy as an increase in the inflow fluctuation intensity. As the shear-layer momentum thickness is decreased, the region of strong growth in the turbulent kinetic energy shifts toward the nozzle from $\approx 6.0h$ to $\approx 3.0h$. For the smallest shear-layer thickness the centerline turbulent kinetic energy grows very strongly and asymptotes rapidly to a value of 0.06. For the thicker shear layers the growth in the turbulent kinetic energy is slower, and an overshoot, with respect to self-similar values reported in experiments and observed in the DNS with $\theta_0/h = 0.025$, occurs near the outflow of the domain.

The overshoot in the centerline turbulent kinetic energy that occurs for the thicker initial shear layers can be related to the rate at which the turbulence approaches an equilibrium state downstream. Figure 9 shows the downstream evolution of the ratio of the turbulent kinetic energy to the dissipation for the jets with differing inflow shear-layer thicknesses. Again, near the inflow the turbulence is highly nonequilibrium. For $\theta_0/h = 0.025$ the fluctuating velocity fields rapidly develop to equilibrium turbulence while for the thicker initial shear layers this evolution is slower. The difference in the evolution of the turbulent fields to equilibrium for a change in the inflow momentum thickness is more dramatic than was observed earlier for variations in the inflow fluctuation intensity. For $\theta_0/h = 0.09$ the fluctuating fields remain highly nonequilibrium until downstream of $x \approx 6.0h$, where there is a very rapid increase in the dissipation relative to the turbulent kinetic energy [indicated by a decrease in $\Delta UK/(\delta_U \epsilon)$]. This is followed by a much slower approach downstream to equilibrium turbulence. This slow approach to equilibrium allows a large overshoot in the turbulent kinetic energy downstream in this jet relative to the jet with $\theta_0/h = 0.025$.

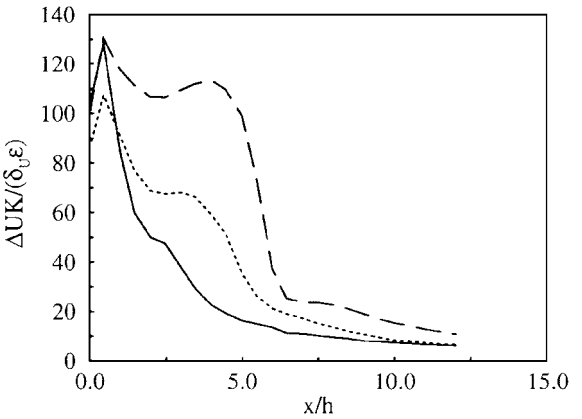

Fig. 9 Downstream evolution of the turbulent kinetic energy to dissipation ratio on the jet centerline for different initial shear-layer momentum thicknesses: ——, $\theta_0/h = 0.025$; - - - -, $\theta_0/h = 0.05$; and – – –, $\theta_0/h = 0.09$.

Influence of Discrete Forcing on the Jet Development

This section discusses the influence of forcing the jet inflow plane using discrete forcing at the shear-layer fundamental and first subharmonic frequencies. Forcing at frequencies associated with the shear layers, rather than the downstream jet mode, is used because the experimental work of Michalke and Freymuth[1] show that the strongest growing modes near the nozzle in natural developing planar jets are those of the shear layer. However, it would be of interest to perform future comparisons with forcing at the jet mode as well. The two discretely forced cases F and G include a broadband forcing at the inflow plane with an intensity of $q_{bb}/\Delta U_0 = 0.05$ superimposed with the two-dimensional discrete forcing with $q_{\text{disc}}/\Delta U_0 = 0.02$ (Table 1). Case F is forced symmetrically with respect to the centerline, whereas case G is forced asymmetrically. Although the broadband intensity is larger, the energy is spread across a large range of scales. The energy in the discrete forcing, on the other hand, is concentrated at only two frequencies (the fundamental and the subharmonic shear-layer modes) and provides roughly an order-of-magnitude larger energy in these modes than is present in the broadband spectrum at the same frequencies.

Figures 10a and 11a show the spanwise vorticity contours on an x/y plane ($z = 0.0h$) and an x/z plane ($y = 0.5h$), respectively, for case A. This case has no discrete forcing and serves as the unforced reference for the two discretely forced cases. For this simulation there are no strong large-scale structures in the flowfield near the nozzle. For simulations with broadband inflow conditions, the strongest growing mode near the jet nozzle is the shear-layer mode (see Ref. 33). However, there is a rapid growth in the energy at all scales because of nonlinear interactions, and no strong large-scale structures appear in the visualization. The wide spacing, in the z direction, between contour lines at $x = 0.0h$ in Fig. 11a, when compared with downstream stations, indicates that the spanwise vorticity contours are relatively two-dimensional near the jet nozzle. However, there is a rapid increase in the three-dimensionality downstream. By $x = 5.0h$ strong small-scale, three-dimensional structures are present in the flowfield.

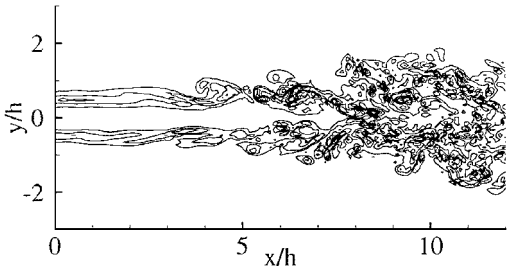

a) Broadband forcing only

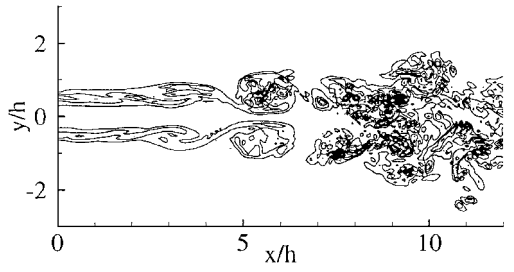

b) Symmetric discrete forcing

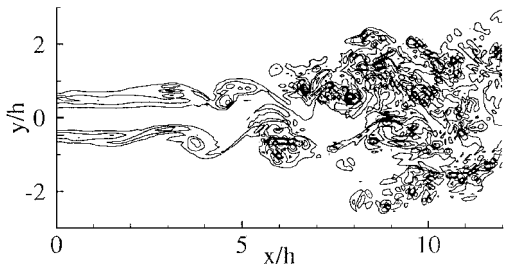

c) Asymmetric discrete forcing

Fig. 10 Spanwise vorticity contours on an *x*/*y* plane ($z = 0.0h$).

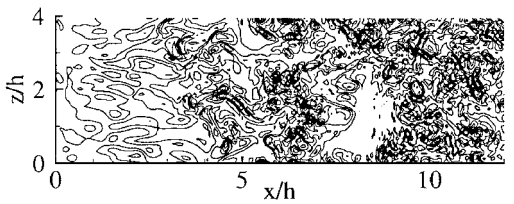

a) Broadband forcing only

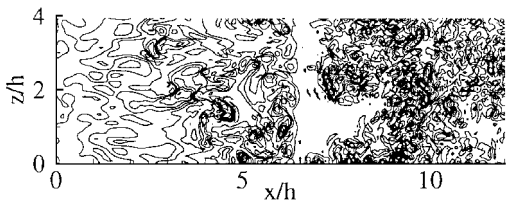

b) Symmetric discrete forcing

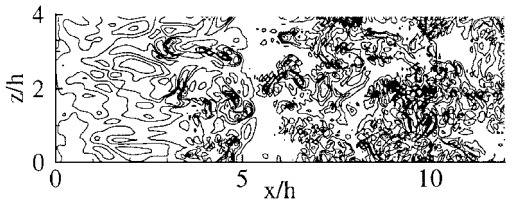

c) Asymmetric discrete forcing

Fig. 11 Spanwise vorticity contours on an *x*/*z* plane in the upper shear layer ($y = 0.5h$).

Figures 10b and 10c show the spanwise vorticity contours on an x/y plane for the symmetrically and asymmetrically forced planar jet simulations, respectively. Although the large-scale structures did not show strongly in the visualization of the vorticity field for the unforced case, for the discretely forced simulations the large-scale structures are very evident. In case F strong symmetrically oriented structures are present in the flowfield in the region $3.0h \leq x \leq 7.0h$, whereas in case G the structures are arranged asymmetrically. Accompanying the large-scale structures in both simulations, there exists a great deal of small-scale three-dimensional structures. Downstream in the jets $x > 7.0h$, there is a strong breakdown of the large-scale structures to small-scale turbulence in both forced simulations.

Figures 11b and 11c show the spanwise vorticity contours on an x/z plane in the upper shear layer for the two discretely forced simulations. Although there is considerable three-dimensionality on the smaller scales, the large-scale structures present in the region $3.0h \leq x \leq 7.0h$ are strongly two-dimensional (indicated by the sharp break between the region of high vorticity and low vorticity at $x = 6.0h$ for all values of z). This is a result of the fact that the discrete forcing at the inflow plane is two-dimensional. In Fig. 11b small-scale three-dimensional structures present within the two-dimensional large-scale vortical structure can be seen in the region $5.0h \leq x \leq 6.0h$. In this region the x/z slice in Fig. 11b passes through the large-scale structure in the upper half of the jet. The breakdown of the two-dimensional large-scale structures downstream is evident in Fig. 11b by the lack of two-dimensionality for $x > 6.0h$. In the region downstream the strong growth in the three-dimensional small-scale turbulent structures overwhelms the two-dimensional forcing at the inflow.

Figures 12 and 13 show the downstream evolution of the centerline velocity decay and the jet half-width for the two discretely

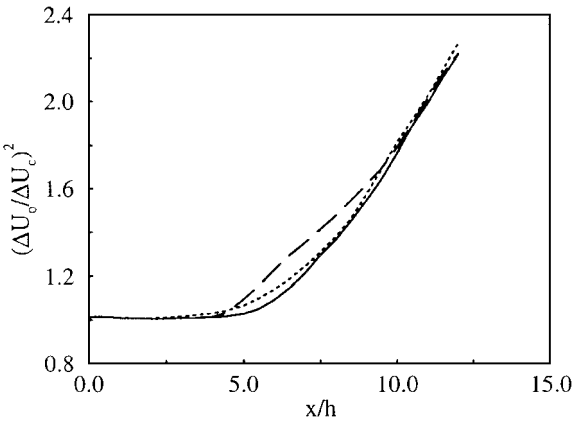

Fig. 12 Downstream evolution of the centerline velocity excess for discretely forced jets: ——, unforced; - - - -, symmetrically forced; and – – –, asymmetrically forced.

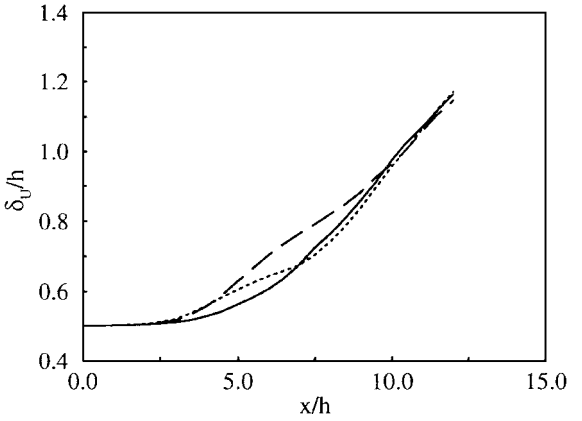

Fig. 13 Downstream evolution of the jet half-width for discretely forced jets: ——, unforced; - - - -, symmetrically forced; and – – –, asymmetrically forced.

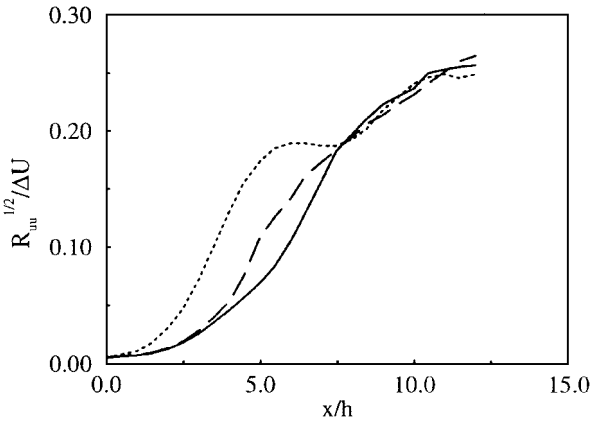

Fig. 14 Downstream evolution of the centerline streamwise fluctuation intensity for forced jets: ——, unforced; - - - -, symmetrically forced; and – – –, asymmetrically forced.

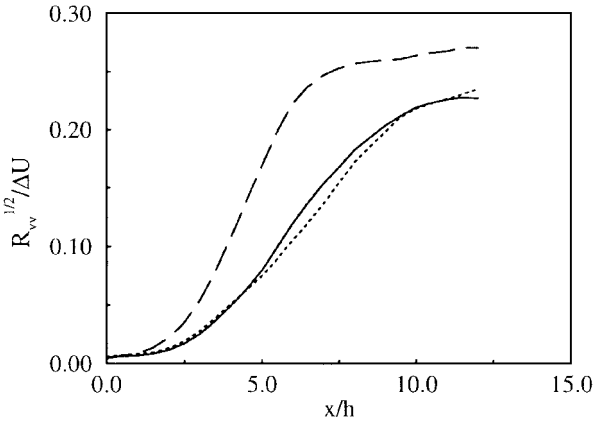

Fig. 15 Downstream evolution of the centerline lateral fluctuation intensity for forced jets: ——, unforced; - - - -, symmetrically forced; and – – –, asymmetrically forced.

forced jets as well as the unforced reference. Although the discrete forcing does influence the jet growth and centerline velocity decay in the region $3.0h \leq x \leq 10.0h$, the effect is relatively small. The strongest effect is observed in the asymmetrically forced jet. Downstream, $x > 10.0h$, and the jet half-width and centerline velocity excess collapse with that of the unforced jet. For the symmetrically forced jet, case F, the effect of forcing is smaller, and the collapse to the unforced behavior occurs more rapidly. Thus, discrete forcing influences the mean fields in the region near the jet nozzle; however, downstream, the mean field does not feel the effect of the inflow forcing.

Although discrete forcing has little influence on the mean streamwise velocity field downstream, it is evident from Fig. 10 that discrete forcing does influence the growth of the vorticity field in the jet. Comparison of Figs. 10a and 10c shows that, for this instant in time, the asymmetric forcing results in an increase in the downstream spread of the vorticity in the jet. This effect results in wider profiles, across the jet, of the turbulent kinetic energy and dissipation for the forced jets compared to the unforced jet. At $x/h = 11.5$ the turbulent kinetic energy profiles, not shown, for the symmetrically and asymmetrically forced jets are 12 and 18% wider, respectively, than the profile for the unforced jet.

Figure 14 shows the downstream evolution of the streamwise Reynolds stress on the jet centerline for the two discretely forced jets as well as the unforced jet. Symmetric forcing at the inflow dramatically increases the growth in the centerline longitudinal Reynolds stress, which is largely an effect of the enforced symmetry of the large-scale structures in the near field of the jet. The influence of the asymmetric forcing on the streamwise Reynolds stress is significantly smaller, although there is some impact in the region $3.0h \leq x \leq 7.0h$. Downstream, the centerline streamwise Reynolds stress for both of the discretely forced jets collapses to that of the unforced jet. There is no significant influence of discrete forcing on the downstream evolution of the streamwise Reynolds stress (not shown here) in the shear layers ($y = \pm 0.5h$).

Figure 15 shows the downstream evolution of the lateral Reynolds stress on the jet centerline for the two discretely forced jets as well as the unforced jet. There is no significant impact of symmetric discrete forcing on the evolution of the centerline lateral Reynolds stress because of the enforced symmetry of the large-scale structures. Symmetric large-scale structures do not impose lateral fluctuations at the centerline of the jet; therefore, turbulent transport of the lateral Reynolds stress from the shear layers is still the dominant means by which the centerline values grow initially. Asymmetric forcing, however, does strongly increase the downstream growth in the lateral Reynolds stress. The asymmetric large-scale structures impose large lateral fluctuations at the centerline of the jet. The lateral Reynolds stress on the centerline for the asymmetrically forced jet peaks rapidly and remains relatively constant through the remainder of the domain. With the domain size used in these simulations, a relaxation of the lateral Reynolds stress in the asymmetrically forced jet back to the unforced values is not observed. In contrast to the streamwise Reynolds stress, both the symmetric and asymmetric forcing cause an increase in the downstream growth of the lateral Reynolds stress (not shown here) in the shear layers ($y = \pm 0.5h$).

There is negligible influence of the symmetric forcing on the spanwise Reynolds stress and only a small influence of asymmetric forcing. This is a result of the two-dimensional nature of the discrete forcing used in this study. It is expected that some energy would transfer from the streamwise and lateral components of the Reynolds stress to the spanwise component through the pressure-strain terms. However, it appears that this effect is small.

Conclusions

Although the flowfield conditions in the shear layers at the nozzle of planar jets are seldom reported in detail, it is clear from the current results that they have a significant impact on the initial development $0.0 < x/h < 10.0$ in these flows. Variations in the broadband fluctuation intensity in the shear layer as well as the shear-layer momentum thickness significantly affect the rate at which the jet develops downstream. This is most strongly felt by an upstream shift in the virtual origins for increasing inflow fluctuation intensity or decreasing shear-layer thickness. This indicates a more rapid evolution of the mean velocity field to self-similar behavior. Likewise, higher fluctuation intensities or thinner shear layers lead to more rapidly developing fluctuating fields with an asymptotic approach of the centerline turbulent kinetic energy to the self-similar values. Thicker shear layers or lower intensity inflow fluctuations result in an overshoot of the centerline turbulent kinetic energy. This overshoot is a result of the initial imbalance between turbulent production and dissipation, characterized by large values of the nondimensional parameter $\Delta U K/\delta_U \epsilon$ for these jets. The self-similar values downstream in the jet are reached when the appropriate balance between the production, dissipation, and transport is achieved. The influence of the shear-layer thickness suggests that the initial development of the jet is dominated by the shear-layer instabilities.

Two-dimensional discrete forcing at the inflow plane of planar turbulent jets has a significant impact on the initial development of the centerline streamwise and lateral Reynolds stresses. This influence, however, appears to be predominantly caused by the enforced symmetry or asymmetry, as well as two-dimensionality, of the large-scale structures near the inflow. Symmetric forcing enhances the growth of the streamwise Reynolds stress with no impact on the lateral Reynolds stress, whereas asymmetric forcing primarily affects the lateral Reynolds stress at the jet centerline. The two-dimensional discrete forcing has only a small effect on the downstream jet growth and centerline velocity decay as well as on the spanwise Reynolds stress. In general, discrete forcing, especially asymmetric forcing, enhances the growth and two-dimensionality of the large-scale structures near the jet nozzle; however, within the interior of the structures significant small-scale three-dimensionality is present. Downstream, these large-scale structures rapidly break down to small-scale turbulence, and the influence of the discrete forcing at the jet centerline is felt only in the lateral Reynolds stress.

The streamwise and spanwise Reynolds stresses on the centerline as well as jet growth and centerline velocity decay rapidly converge to values corresponding to the unforced jet downstream. However, both symmetric and asymmetric forcing of the jet produce considerable widening of the turbulent kinetic energy profiles downstream, $x = 11.5h$.

Acknowledgments

Support for the first author was provided by the Applied Mathematical Sciences Program of the Department of Energy Office of Mathematics, Information, and Computational Sciences under contract DE-AC03-76SF00098 as well as by the Department of Energy Computational Sciences Graduate Fellowship Program. Partial support for the second author was provided by the Office of Naval Research through Grant ONR N00014-99-1-0745. This work was supported in part by a grant of high-performance computing time from the Naval Oceanographic Office Department of Defense Major Shared Resource Center. In addition, this research used resources of the National Energy Research Scientific Computing Center, which is supported by the Office of Energy Research of the U.S. Department of Energy.

References

[1]Michalke, A., and Freymuth, P., "The Instability and the Formation of Vortices in a Free Boundary Layer," *Separated Flows, Part 2*, AGARD Conf. Proceedings 4, AGARD, Paris, 1966, pp. 575–595.

[2]Sato, H., "The Stability and Transition of a Two-Dimensional Jet," *Journal of Fluid Mechanics*, Vol. 7, No. 1, 1960, pp. 53–80.

[3]Rockwell, D. O., and Niccolls, W. O., "Natural Breakdown of Planar Jets," *Journal of Basic Engineering*, Vol. 94, No. 4, 1972, pp. 720–730.

[4]Antonia, R. A., Browne, L. W. B., Rajagopalan, S., and Chambers, A. J., "On the Organized Motion of a Turbulent Plane Jet," *Journal of Fluid Mechanics*, Vol. 134, 1983, pp. 49–66.

[5]Bradbury, L. J. S., "The Structure of a Self-Preserving Turbulent Plane Jet," *Journal of Fluid Mechanics*, Vol. 23, No. 1, 1965, pp. 31–64.

[6]Gutmark, E., and Wygnanski, I., "The Planar Turbulent Jet," *Journal of Fluid Mechanics*, Vol. 73, No. 3, 1976, pp. 465–495.

[7]Ramaprian, B. R., and Chandrasekhara, M. S., "LDA Measurements in Plane Turbulent Jets," *Journal of Fluids Engineering*, Vol. 107, No. 2, 1985, pp. 264–271.

[8]Oler, J. W., and Goldschmidt, V. W., "Interface Crossing Frequency as a Self-Preserving Flow Variable in a Turbulent Plane Jet," *Physics of Fluids*, Vol. 23, No. 1, 1980, pp. 19–21.

[9]Oler, J. W., and Goldschmidt, V. W., "A Vortex-Street Model of the Flow in the Similarity Region of a Two-Dimensional Free Turbulent Jet," *Journal of Fluid Mechanics*, Vol. 123, 1982, pp. 523–535.

[10]Mumford, J. C., "The Structure of the Large Eddies in Fully Developed Turbulent Shear Flows Part 1: The Plane Jet," *Journal of Fluid Mechanics*, Vol. 118, 1982, pp. 241–268.

[11]Thomas, F. O., and Goldschmidt, V. W., "Acoustically Induced Enhancement of Widening and Fluctuation Intensity in a Two-Dimensional Turbulent Jet," *Journal of Fluids Engineering*, Vol. 108, No. 3, 1986, pp. 331–337.

[12]Thomas, F. O., and Goldschmidt, V. W., "Structural Characteristics of a Developing Turbulent Planar Jet," *Journal of Fluid Mechanics*, Vol. 163, 1986, pp. 227–256.

[13]Thomas, F. O., and Chu, H. C., "An Experimental Investigation of the Transition of a Planar Jet: Subharmonic Suppression and Upstream Feedback," *Physics of Fluids A*, Vol. 1, No. 9, 1989, pp. 1566–1587.

[14]Thomas, F. O., and Prakash, K. M. K., "An Experimental Investigation of the Natural Transition of an Untuned Planar Jet," *Physics of Fluids A*, Vol. 3, No. 1, 1991, pp. 90–105.

[15]Namer, I., and Ötügen, M. V., "Velocity Measurements in a Plane Turbulent Air Jet at Moderate Reynolds Numbers," *Experiments in Fluids*, Vol. 6, 1988, pp. 387–399.

[16]Hill, W. G., Jr., and Jenkins, R. C., "Effects of the Initial Boundary-Layer State on Turbulent Jet Mixing," *AIAA Journal*, Vol. 14, No. 11, 1976, pp. 1513, 1514.

[17]Comte, P., Lesieur, M., Laroche, H., and Normand, X., "Numerical Simulations of Turbulent Plane Shear Layers," *Turbulent Shear Flows 6*, edited by J.-C. André, J. Cousteix, F. Durst, B. E. Launder, F. W. Schmidt, and J. H. Whitelaw, Springer-Verlag, Berlin, 1989, pp. 361–380.

[18]Reichert, R. S., and Biringen, S., "Numerical Simulation of Compressible Plane Jets," AIAA Paper 97-1924, June 1997.

[19]Dai, Y., Kobayashi, T., and Taniguchi, N., "Large Eddy Simulation of Plane Turbulent Jet Flow Using a New Outflow Velocity Boundary Condition," *JSME International Journal Series B-Fluids and Thermal Engineering*, Vol. 37, No. 2, 1994, pp. 242–253.

[20]Weinberger, C., Rewerts, J., and Janicka, J., "The Influence of Inlet Conditions on a Large Eddy Simulation of a Turbulent Plane Jet," *Proceedings of the 11th Symposium on Turbulent Shear Flows*, Vol. 3, Springer-Verlag, Grenoble, France, 1997, pp. 25.17–25.22.

[21]Le Ribault, C., Sarkar, S., and Stanley, S. A., "Large Eddy Simulation of a Plane Jet," *Physics of Fluids* (submitted for publication).

[22]Carpenter, M. H., and Kennedy, C. A., "Fourth-Order 2N-Storage Runge–Kutta Schemes," NASA TM 109112, June 1994.

[23]Lele, S. K., "Compact Finite Difference Schemes with Spectral-Like Resolution," *Journal of Computational Physics*, Vol. 103, No. 1, 1992, pp. 16–42.

[24]Carpenter, M. H., Gottlieb, D., and Abarbanel, S., "The Stability of Numerical Boundary Treatments for Compact High-Order Finite-Difference Schemes," *Journal of Computational Physics*, Vol. 108, 1993, pp. 272–295.

[25]Gamet, L., Ducros, F., Nicoud, F., and Poinsot, T., "Compact Finite Difference Schemes on Non-Uniform Meshes. Application to Direct Numerical Simulations of Compressible Flows," *International Journal of Numerical Methods in Fluids*, Vol. 29, No. 2, 1999, pp. 159–191.

[26]Thompson, K. W., "Time Dependent Boundary Conditions for Hyperbolic Systems," *Journal of Computational Physics*, Vol. 68, No. 1, 1987, pp. 1–24.

[27]Thompson, K. W., "Time-Dependent Boundary Conditions for Hyperbolic Systems II," *Journal of Computational Physics*, Vol. 89, No. 2, 1990, pp. 439–461.

[28]Rudy, D. H., and Strikwerda, J. C., "A Nonreflecting Outflow Boundary Condition for Subsonic Navier–Stokes Calculations," *Journal of Computational Physics*, Vol. 36, No. 1, 1980, pp. 55–70.

[29]Poinsot, T. J., and Lele, S. K., "Boundary Conditions for Direct Simulations of Compressible Viscous Flows," *Journal of Computational Physics*, Vol. 101, No. 1, 1992, pp. 104–129.

[30]Hu, F. Q., "On Absorbing Boundary Conditions for Linearized Euler Equations by a Perfectly Matched Layer," *Journal of Computational Physics*, Vol. 129, No. 1, 1996, pp. 201–219.

[31]Michalke, A., "On Spatially Growing Disturbances in an Inviscid Shear Layer," *Journal of Fluid Mechanics*, Vol. 23, No. 3, 1965, pp. 521–544.

[32]Monkewitz, P. A., and Huerre, P., "Influence of the Velocity Ratio on the Spatial Instability of Mixing," *Physics of Fluids*, Vol. 25, No. 7, 1982, pp. 1137–1143.

[33]Stanley, S. A., and Sarkar, S., "A Study of the Flowfield Evolution and Mixing in a Planar Turbulent Jet Using Direct Numerical Simulation," *Journal of Fluid Mechanics* (submitted for publication).

[34]Stanley, S. A., and Sarkar, S., "Direct Numerical Simulation of the Developing Region of Turbulent Planar Jets," AIAA Paper 99-0288, Jan. 1999.

[35]Stanley, S., and Sarkar, S., "Simulations of Spatially Developing Two-Dimensional Shear Layers and Jets," *Theoretical and Computational Fluid Dynamics*, Vol. 9, No. 2, 1997, pp. 121–147.

[36]Hussain, A. K. M. F., and Zedan, M. F., "Effects of the Initial Conditions on the Axisymmetric Free Shear Layer: Effect of the Initial Fluctuation Level," *Physics of Fluids*, Vol. 21, No. 9, 1978, pp. 1475–1481.

[37]Browne, L. W. B., Antonia, R. A., Rajagopalan, S., and Chambers, A. J., "Interaction Region of a Two-Dimensional Turbulent Plane Jet in Still Air," *Structure of Complex Turbulent Shear Flow*, edited by R. Dumas and L. Fulachier, Springer-Verlag, Berlin, 1983, pp. 411–419.

[38]Hussain, A. K. M. F., and Zedan, M. F., "Effects of the Initial Conditions on the Axisymmetric Free Shear Layer: Effects of the Initial Momentum Thickness," *Physics of Fluids*, Vol. 21, No. 7, 1978, pp. 1100–1112.

[39]George, W. K., "The Self-Preservation of Turbulent Flows and Its Relation to Initial Conditions and Coherent Structures," *Advances in Turbulence*, edited by W. K. George and R. Arndt, Hemisphere, New York, 1989, pp. 39–73.

K. Kailasanath
Associate Editor